EDGEWOOD

CHEMICAL BIOLOGICAL CENTER

U.S. ARMY RESEARCH, DEVELOPMENT AND ENGINEERING COMMAND

ECBC-TR-835

OPTICAL, PHYSICAL, AND CHEMICAL PROPERTIES OF SURFACE MODIFIED TITANIUM DIOXIDE POWDERS

Brendan G. DeLacy

RESEARCH AND TECHNOLOGY DIRECTORATE

David R. Redding

ENGINEERING DIRECTORATE

Joshua Matthews

SCIENCE APPLICATIONS
INTERNATIONAL CORPORATION
Gunpowder, MD 21010-0068

February 2011

ABERDEEN PROVING GROUND, MD 21010-5424

Disclaimer

The findings in this report are not to be construed as an official Department of the Army position unless so designated by other authorizing documents.

REPORT DOCUMENTATION PAGE

Form Approved
OMB No. 0704-0188

1. REPORT DATE *(DD-MM-YYYY)*	2. REPORT TYPE	3. DATES COVERED *(From - To)*
XX-02-2011	Final	Apr 2008 - Dec 2009

4. TITLE AND SUBTITLE
Optical, Physical, and Chemical Properties of Surface Modified Titanium Dioxide Powders

5a. CONTRACT NUMBER

5b. GRANT NUMBER

5c. PROGRAM ELEMENT NUMBER

6. AUTHOR(S)
DeLacy, Brendan G.; Redding, David R. (ECBC); and Matthews, Joshua (SAIC)

5d. PROJECT NUMBER
62622A552

5e. TASK NUMBER

5f. WORK UNIT NUMBER

7. PERFORMING ORGANIZATION NAME(S) AND ADDRESS(ES)
DIR, ECBC, ATTN: RDCB-DRT-S/RDCB-DPO-S, APG, MD 21010-5424
SAIC, P.O. Box 68, Gunpowder, MD 21010-0068

8. PERFORMING ORGANIZATION REPORT NUMBER
ECBC-TR-835

9. SPONSORING / MONITORING AGENCY NAME(S) AND ADDRESS(ES)
JPM Reconnaissance and Platform Integration, APG, MD 21010-5424

10. SPONSOR/MONITOR'S ACRONYM(S)

11. SPONSOR/MONITOR'S REPORT NUMBER(S)

12. DISTRIBUTION / AVAILABILITY STATEMENT
Approved for public release; distribution is unlimited.

13. SUPPLEMENTARY NOTES

14. ABSTRACT-LIMIT 200 WORDS

Titanium Dioxide (TiO_2) powder is currently used by the U.S. Army as an obscurant fill in the M82 and M106 visible smoke grenades. The U.S. Army previously evaluated a wide range of TiO_2 powders for use in these grenades. However, the chemical and physical properties of these powders were not explored in the context of grenade performance. Therefore, an initial study was undertaken to characterize the chemical, physical, and optical properties of TiO_2 powders that impact its performance in the M106 grenade. A desired outcome of the study is to incorporate the requisite characteristics into product specifications, thereby improving the performance of the M106.

15. SUBJECT TERMS

Mass Extinction	Carr Indices	Contact Angle	Mie Theory
Refractive Index	Laser Diffraction	Surface Area	Titanium Dioxide
Dissemination Yield	Organosilanes		

16. SECURITY CLASSIFICATION OF:			17. LIMITATION OF ABSTRACT	18. NUMBER OF PAGES	19a. NAME OF RESPONSIBLE PERSON
a. REPORT	b. ABSTRACT	c. THIS PAGE			Sandra J. Johnson
U	U	U	UL	46	19b. TELEPHONE NUMBER *(include area code)* (410) 436-2914

Blank

PREFACE

The work described in this report was authorized under Project No. 62622A552 for the JPM Reconnaissance and Platform Integration Team. This work was started in April 2008 and completed in December 2009.

The use of either trade or manufacturers' names in this report does not constitute an official endorsement of any commercial products. This report may not be cited for purposes of advertisement.

This report has been approved for public release. Registered users should request additional copies from the Defense Technical Information Center; unregistered users should direct such requests to the National Technical Information Service.

Acknowledgments

The authors acknowledge Frank Bagala of Package Kare (Middlesex, NJ) for his assistance in running the Gemco blender and Dr. Chip Cody of JEOL (Peabody, MA) for his evaluation of coatings using Accu-Time of Flight Direct Analysis in Real Time (TOF-DART) mass spectrometry.

Blank

CONTENTS

FIGURES

TABLES

Blank

OPTICAL, PHYSICAL, AND CHEMICAL PROPERTIES OF SURFACE MODIFIED TITANIUM DIOXIDE POWDERS

1. INTRODUCTION

Titanium Dioxide (TiO_2) powder is currently used by the U.S. Army as an obscurant fill in the M82 and M106 visible smoke grenades. The Army previously evaluated a wide range of TiO_2 powders for use in these grenades. However, the chemical and physical properties of these powders were not explored in the context of grenade performance. Therefore, an initial study was undertaken to characterize the chemical, physical, and optical properties of TiO_2 powders that impact its performance in the M106 grenade. A desired outcome of the study is to incorporate the requisite characteristics into product specifications, thereby improving the performance of the M106.

TiO_2 is well known for its scattering properties in the visible region of the electromagnetic spectrum. The tendency of TiO_2 to attenuate visible light is largely due to its high refractive index. The attenuation properties of TiO_2 in the visible region are also strongly dependent on the particle size of the material. Theoretical calculations based on Mie theory predict that the optimum particle size of TiO_2 for attenuating UV visible light is approximately 0.20 μm.[1]

Multiple manufacturers of TiO_2 produce powders with grain sizes that are near 0.20 μm. Imaging using scanning electron microscopy (SEM) confirms this claim. However, in the dry powdered state, TiO_2 powders tend to exhibit significantly larger particle sizes due to agglomeration. TiO_2 powders are often coated to lower the surface energy of the particles and to minimize inter-particle forces. The coating chosen for the powder is largely dependent on the application of the material. For example, a suspension of TiO_2 particles in an aqueous solvent requires a hydrophilic coating. Conversely, a hydrophobic coating would be more suitable for suspension in a hydrophobic polymeric substrate. The use of TiO_2 powder as an aerosolized obscurant is a unique application. Hence, an understanding of coatings and additives used by manufacturers of TiO_2 and their impact on the dispersion as a powder is integral to understanding the use of TiO_2 as a visible obscurant.

To explore the impact of coatings on obscuration performance, the extinction properties of multiple grades of commercially available TiO_2 were evaluated in the U.S. Army Edgewood Chemical Biological Center (ECBC) aerosol chamber. Each product was disseminated pneumatically through a sonic nozzle and explosively using the M106 grenade. Chamber evaluation involved the determination of mass extinction, yield, and deposition rate. The products evaluated in this study were obtained from DuPont (Wilmington, DE), Millennium (Glen Burnie, MD), and Tronox Corporation (Oklahoma City, OK). These corporations manufacture different grades of TiO_2 that vary in purity, coatings, inorganic content (alumina, silica, zirconia), and organic treatment. In addition to the chamber tests, contact angle, surface energy, SEM, flow characteristic measurements, and mass spectrometry analysis were performed. The purpose of these tests was to determine if there was any correlation between the physical or chemical properties of the powders and the obscuration results obtained from the chamber.

In addition to the testing of commercially available grades of TiO_2 powders, an in-house study exploring the impact of coatings on screening performance was also undertaken. This involved coating Millennium lot RCL-9 with a range of silanes and polyols. RCL-9 was chosen as a substrate for its high purity and absence of organic treatment. The experimentally coated powders underwent the same tests as the commercially available products. Namely, mass extinction, yield, contact angle, surface energy, SEM, and flow characteristics measurements were performed.

2. THEORETICAL BACKGROUND OF TIO_2 SCATTERING

An image observed through an aerosol cloud consists of the transmitted original image, attenuated by scatter and absorption, plus ambient light scattered or emitted along the line of sight within the cloud (path radiance) and superimposed onto the transmitted image. Contrast transmittance through the cloud is frequently used to quantify these two effects upon visibility through a cloud. It is defined as the ratio of image contrast as seen through a cloud divided by image contrast without the cloud present and is a function of extinction coefficient, single scatter albedo, asymmetry parameter, concentration path length product, emission and ambient illumination.[2] Extinction is defined in terms of the beam attenuation of electromagnetic radiation due to scattering and absorption as it traverses a medium. Extinction properties of a two phase system such as an aerosol depend on the complex refractive index, size, shape, orientation and number concentration of the particles, complex refractive index of the particles relative to that of the surrounding medium, as well as wavelength and polarization of the incident radiation.[3] The extinction coefficient, α, is related to the beam transmittance T through an aerosol cloud by eq 1:

$$T = e^{-\int \alpha c \, dl} \tag{1}$$

Where c is the concentration of particles along the line of sight and dl is the path length increment. Assuming constant extinction coefficient along the path length for a cloud containing one aerosol material of uniform particle composition and size distribution, the concentration path length integral can be written as any combination of constant concentration and path length yielding that product. Chamber aerosol measurements involve a uniform concentration and known path length. Aerosol extinction is conveniently expressed as a mass extinction coefficient in units of meters^2/gram when calculated from measurements of beam transmittance over a path length specified in meters through an aerosol with uniform mass concentration specified in units of gram/meters^3.

The mass extinction coefficient depends on the optical efficiency factor, Q_{ext}, the geometric cross section, G, and the particle mass as indicated by the relationship in eq 2:

$$\alpha = \frac{Q_{ext} G}{particle\ mass} \tag{2}$$

Generally numerical solutions for Q_{ext} are obtained using Mie calculations for homogeneous spherical particles.[3] Mie theory describes the interaction of light of wavelength λ

with a homogeneous spherical particle of radius a. The relationship between the efficiency factor, Q_{ext}, and the extinction cross section, C_{ext} is described by eq 3:

$$C_{ext} = Q_{ext} \cdot G \tag{3}$$

The Mie solution for the extinction cross section of a sphere, C_{ext}, is given by eq 4:

$$C_{ext} = \frac{2\pi}{k^2}\sum_{n=1}^{n=\infty}(2n+1)\mathrm{Re}\left(|a_n|^2 + |b_n|^2\right) \tag{4}$$

Where the scattering coefficients a_n and b_n must first be determined via eqs 5 and 6:

$$a_n = \frac{\left[D_n(mx)/m + n/x\right]\psi_n(x) - \psi_{n-1}(x)}{\left[D_n(mx)/m + n/x\right]\xi_n(x) - \xi_{n-1}(x)} \tag{5}$$

$$b_n = \frac{\left[mD_n(mx)/m + n/x\right]\psi_n(x) - \psi_{n-1}(x)}{\left[mD_n(mx)/m + n/x\right]\xi_n(x) - \xi_{n-1}(x)} \tag{6}$$

Here, x is the size parameter and m is the relative refractive index described by eqs 7 and 8:

$$x = ka = \frac{2\pi Na}{\lambda} \tag{7}$$

$$m = \frac{N_1}{N} \tag{8}$$

N_1 and N are the refractive indices of the particle and medium, respectively. Ψ and ξ are Riccati-Bessel functions, where the recurrence relations are illustrated by eqs 9 and 10:

$$\psi_n'(x) = \psi_{n-1}(x) - \frac{n\psi_n(x)}{x} \tag{9}$$

$$\xi_n'(x) = \xi_{n-1}(x) - \frac{n\xi_n(x)}{x} \tag{10}$$

These are satisfied by the logarithmic derivative, D_n, described by eq 11:

$$D_{n-1} = \frac{n}{\rho} - \frac{1}{D_n + n/\rho} \tag{11}$$

Figure 1 is a plot of the theoretical mass extinction coefficients (MECs) for a range of TiO_2 particle sizes (120 nm-240 nm) using the Mie theory. The MECs were calculated in the visible region and a refractive index of 2.74 was assumed. Averaged over the visible

region, the MECs for both the 200 nm and 220 nm particle sizes are 8.1 m^2/g. Hence, a mean particle size of ~220 nm is required for maximizing attenuation in the visible region.

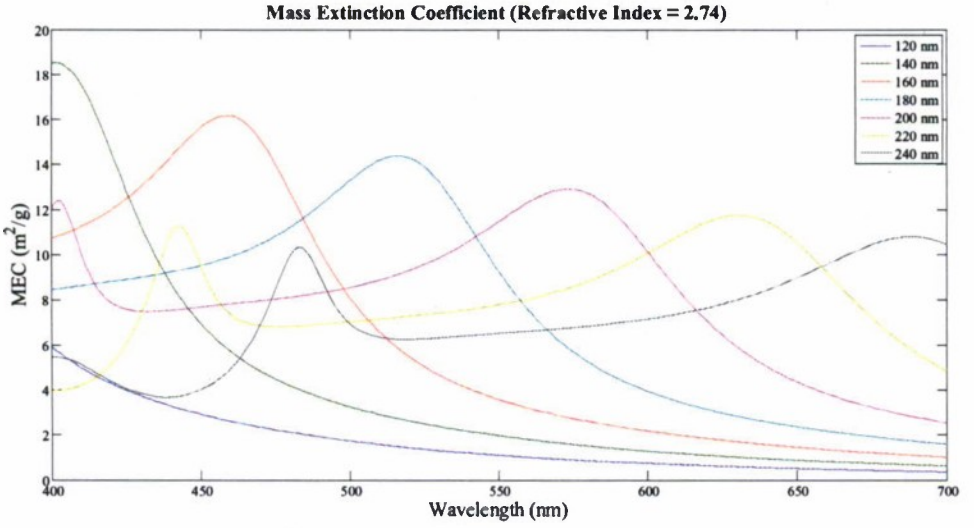

Figure 1 - Theoretical Mass Extinction Coefficient for a Range of TiO_2 Particle Sizes

3. EXPERIMENTAL DETERMINATION OF EXTINCTION COEFFICIENT AND DISSEMINATION EFFICIENCY

When determining the extinction coefficient and dissemination efficiency of a given material experimentally, a range of parameters must be considered. First, the mass extinction of a given powder may be determined via the Beer-Lambert Law shown by eq 12:

$$\alpha\left[m^2/g\right] = \frac{-\ln(T)}{C \cdot L} \tag{12}$$

Where T is the transmission, C is the concentration in m^2/g, and L is the path length. Determination of mass extinction can be made in a controlled environment such as a chamber where the path length is held constant and transmission and concentration may be determined.

Dissemination efficiency of the powder is another consideration. Dry powders may be aerosolized using a pneumatic re-dispersion technique in which a powder is loosely fed into an air stream and subsequently dispersed through a nozzle.[4] Alternatively, a dry powder can be disseminated explosively by filling the dry powder concentrically around a center charge of explosive.[5]

Dissemination techniques used to produce an aerosol cloud play a vital role in aerosol dispersion and degree of agglomeration. Characterization of the dissemination method performance is generally summed up with two measurements: yield and particle size distribution.

As long as particle sizes do not significantly impact cloud lifetimes of interest, particle size measurements can be avoided and measurement of the extinction coefficient suffices. Yield, a measure of dissemination efficiency, is defined as the ratio of the mass aerosolized to the mass of material that entered the dissemination device (eq 13):

$$Yield = \frac{mass\ of\ airborne\ material}{initial\ mass\ of\ material} \tag{13}$$

For explosive dissemination, a metric that encompasses the material performance in addition to the device performance is required. The grenade figure of merit is a metric which encompasses both of these attributes. The grenade figure of merit is defined in eq 14:

$$Figure\ of\ Merit = (\alpha \cdot \rho \cdot Fill\ Factor \cdot Yield) \tag{14}$$

Where, α is the extinction in meters^2/gram, ρ is the material density in g/cm^3, fill factor is the ratio of packed density to the intrinsic material density, and yield is the ratio of airborne mass to initial mass of material in grenade.

In addition to yield, figure of merit, and particle size, deposition rate is a parameter which is descriptive of the aerosol size, mass, and shape. The stirred settling model for a cylindrical chamber with height H and volume V, relates the aerosol deposition velocity, v_D, to the rate of change of aerosolized mass, m via eq 15:

$$\frac{dm}{dt} = -v_D \cdot A \cdot C \tag{15}$$

Where A is the base area of the chamber and C is the concentration of aerosol. The aerosol mass may be expressed as eq 16:

$$m = C \cdot V \tag{16}$$

Substitution yields the following (eq 17):

$$\frac{d(CV)}{dt} = -v_D AC \tag{17}$$

Assuming a constant chamber volume, eq 17 yields (eq 18):

$$\frac{dC}{C} = \frac{-v_D A}{V} dt = -v_D \frac{dt}{H} \tag{18}$$

This has the solution given in eq 19:

$$C = C_0 e^{-v_D t / H} \tag{19}$$

Therefore, the deposition velocity v_D may be deduced from the stirred settling theory by making two filter sample concentration measurements, c_1, and c_2 by way of eq 20:

$$v_D = \frac{H}{t_2 - t_1} \ln(c_1/c_2) \quad (20)$$

The spherical diameter of the particle, d, can subsequently be deduced from the relationship given in eq 21:

$$v_D = \frac{\rho_P d^2 g}{18\eta} \quad (21)$$

Where ρ_P is the density of the particle, g is the acceleration due to gravity, and η is the viscosity of air.

4. CHAMBER MEASUREMENTS OF COMMERCIALLY AVAILABLE TIO_2 POWDERS

To evaluate the performance of a wide range of TiO_2 powders, 15 grades of commercially available TiO_2 powders were tested in the ECBC aerosol chamber. These grades varied in purity, coatings, organic, and inorganic content. A description of the commercially available powders is provided in Table 1.

Table 1 - Commercially Available TiO_2 Powders Tested

Lot #	Manufacture	TiO_2 Purity	Inorganic Coating	Organic Treatment
R700	DuPont	96%	Alumina	Present
R706	DuPont	93%	Alumina, Silica	Present
R900	DuPont	94%	Alumina	None
R931	DuPont	80%	Alumina, Silica	None
R101	DuPont	97%	Alumina	Present
Tiona 595	Millennium	95%	Alumina, Zirconia	Present
Tiona 596	Millennium	94%	Aluminum Hydroxide, Silica	Present
Tiona 188	Millennium	98.5	Aluminum Hydroxide	Present
Tiona RCL-9	Millennium	94%	Alumina	None
Tiona RCL-4	Millennium	97%	Alumina	Present
CR-470	Tronox	97%	Alumina, Silica	Present
CR-813	Tronox	86%	Alumina, Silica	None
CR-826	Tronox	93%	Alumina, Silica	None
CR-834	Tronox	97%	Alumina	None

A diagram of the chamber, in which all the tests were performed, is provided in Figure 2. The ECBC aerosol chamber is a cylindrical chamber with a volume of 190 m^3 (6 m diameter, 6.8 m height). It is equipped with a stirring fan to provide a homogeneous mixture of aerosols throughout. Transmission in the visible region 300 to 900 nm was achieved with an

Ocean Optics UV/Vis spectrometer (Model HR2000CG-UV-NIR, Dunedin, FL). Transmission in the infrared region (0.9 to 20 μm) was determined using two Jasco FTIR spectrometers (Model FT/IR-6100, Jasco Inc., Easton, MD). A path length of 6 m was used in all calculations as the visible and FTIR sources were placed 6 m away from the detectors. The FTIR source and detector were placed at a height of 3.4 m. The concentration of flake material within the chamber was determined by taking an aliquot of air from the chamber. This was achieved by pulling air samples from the chamber onto a glass filter for a 120 s. The mass accumulated on the filter was weighed and the volume of air sampled during filtration was measured using a flow meter (Model FMA-1618A, Omega Engineering, Inc., Stamford, CT). It should be noted that transmission and concentration were not measured until homogeneity in the chamber was achieved after dissemination. Homogeneity was assumed when a steady state in laser transmission was observed. A 672 nm laser diode (Newport, Mountain View, CA) was used in the laser transmissometer system.

All powders were disseminated and tested using two different techniques. First, each powder was disseminated pneumatically and tested in triplicate using a Stanford Research Institute (SRI, Menlo Park, CA) sonic nozzle (outlet pressure = 90 psi). Next, each powder was disseminated explosively and tested in triplicate using the M106 grenade. Extinction, yield, and calculated particle diameters of the pneumatically and explosively disseminated commercial powders are provided in Tables 2 and 3, respectively. Additionally, the fill fraction and grenade figures of merit values are provided for the explosive dissemination tests.

Table 2 - SRI Nozzle Dissemination Chamber Results

Material	Extinction (0.4–0.7 μm)	SD	Yield	Calculated Particle Size (μm)
Tiona 188	4.26	0.32	0.90	2.1
Tiona 595	3.70	0.40	0.81	2.3
Tiona 596	3.35	0.14	0.92	3.1
Tiona RCL-4	3.47	0.05	0.82	2.8
Tiona RCL-9	3.35	0.14	1.03	1.6
R101	2.77	0.09	0.84	2.3
R700	3.29	0.24	1.03	3.3
R706	3.33	0.08	0.77	2.4
R900	2.55	0.08	1.01	2.3
R931 W26	2.87	0.07	0.99	2.2
CR-470	3.79	0.02	0.95	1.6
CR-813	2.73	0.06	1.03	1.4
CR-826	2.54	0.07	0.94	1.8
CR-834	2.83	0.26	0.97	3.0

SD = Standard Deviation, SRI = Stanford Research Instruments

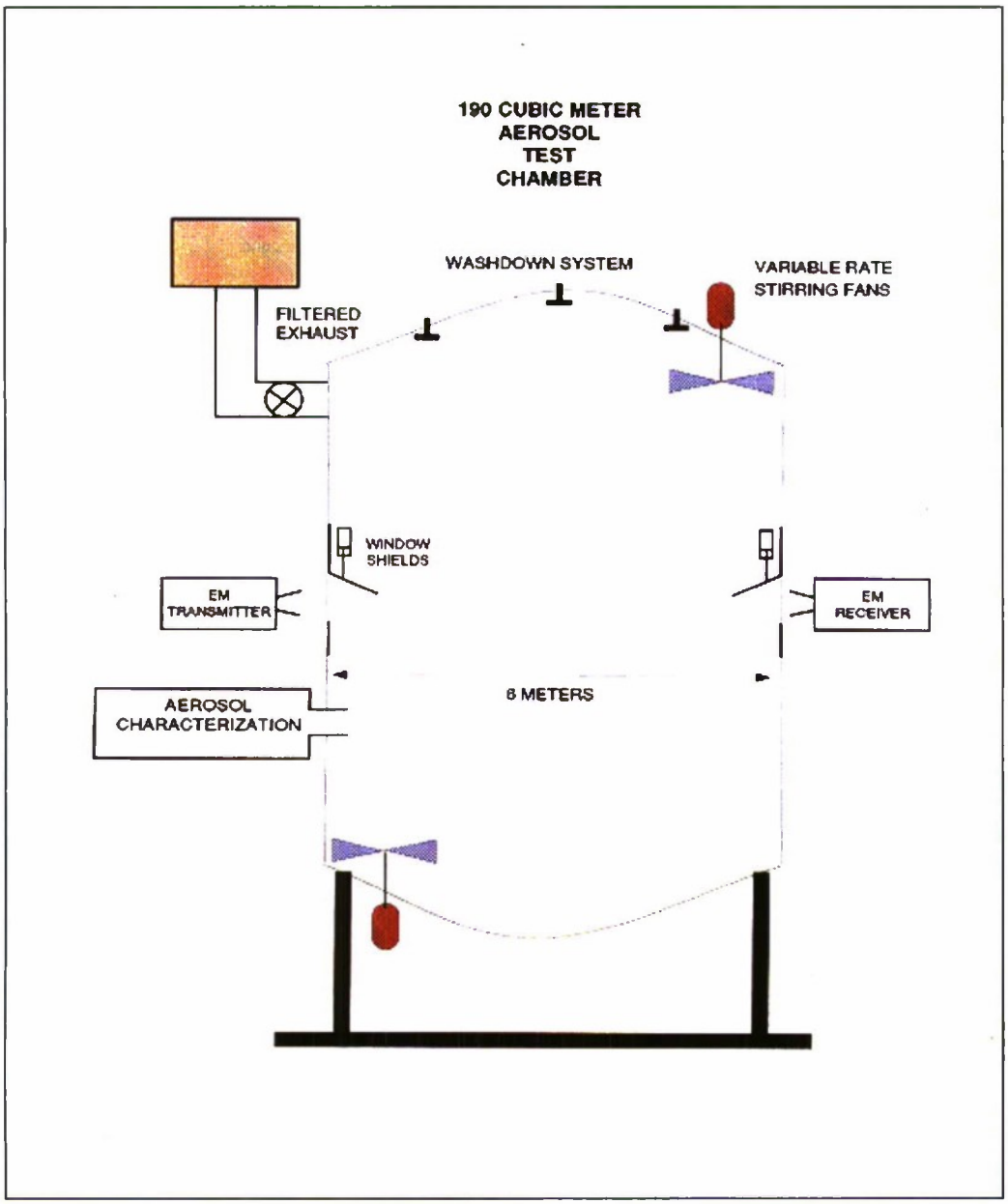

Figure 2 - ECBC Aerosol Chamber

Table 3 - Explosive Dissemination Chamber Results

Material	Extinction (0.4-0.7 μm)	SD	Yield	Calculated Particle Size (μm)	Fill Fraction	Figure of Merit
Tiona 188	1.97	0.15	0.14	7.3	0.29	0.34
Tiona 595	1.62	0.05	0.15	6.9	0.30	0.31
Tiona 596	1.70	0.11	0.16	6.3	0.27	0.31
Tiona RCL-4	1.51	0.17	0.11	8.0	0.32	0.22
Tiona RCL-9	1.11	0.14	0.15	7.4	0.27	0.19
R101	1.54	0.20	0.08	7.3	0.22	0.11
R700	1.83	0.11	0.13	6.6	0.29	0.29
R706	1.56	0.04	0.19	6.9	0.30	0.38
R900	1.64	0.09	0.12	7.3		
R931 W26	1.20	0.13	0.17	7.2	0.17	0.15
CR-470	2.10	0.09	0.23	7.1	0.31	0.63
CR-813	1.24	0.04	0.21	7.5	0.18	0.20
CR-826	1.72	0.12	0.16	6.4	0.26	0.30
CR-834	1.83	0.07	0.15	7.3	0.26	0.30

SD = Standard Deviation, v_D = deposition velocity

5. SURFACE MODIFICATION OF TiO_2

Each of the commercial powders tested in the aerosol chamber exhibited unique obscuration properties, which are greatly influenced by the surface coatings used in their manufacturing process. Coatings play a vital role in the prevention of agglomeration and control of particle size. In order to gain a greater understanding of which coatings impact the obscuration properties of TiO_2 powders, a series of coating studies were conducted.

TiO_2, like other oxides of aluminum, zirconium, and nickel are amenable to surface modification with organosilanes. These surface modifiers can create either a hydrophobic surface or hydrophilic surface, depending upon the chosen organosilane. The general formula of an organosilane is:

$$R_nSiX_{(4-n)} \tag{22}$$

Here X is a hydrolyzable group such as an alkoxy, amine, or halogen and R is an alkyl group. If the hydrolyzable group is an alkoxy, the rate of hydrolysis is inversely proportional to the size of

the alkoxy group. The rate of hydrolysis is also decreased with a decrease in the number of alkoxy substitutions.

Upon hydrolysis, silanol groups (-SiOH) are formed, which can subsequently condense with other silanol or hydroxyl groups on the surface of particles. Typically, condensation first occurs between silanol groups of adjacent organosilanes producing oligomers.[6] The oligomers subsequently form hydrogen bonds with the hydroxyl groups that are present on a substrate surface or particle. Covalent bonds between the oligomer and substrate are finally formed via further condensation and curing. A mechanism for the reactions of an alkyltrimethoxysilane is provided in Figure 3.

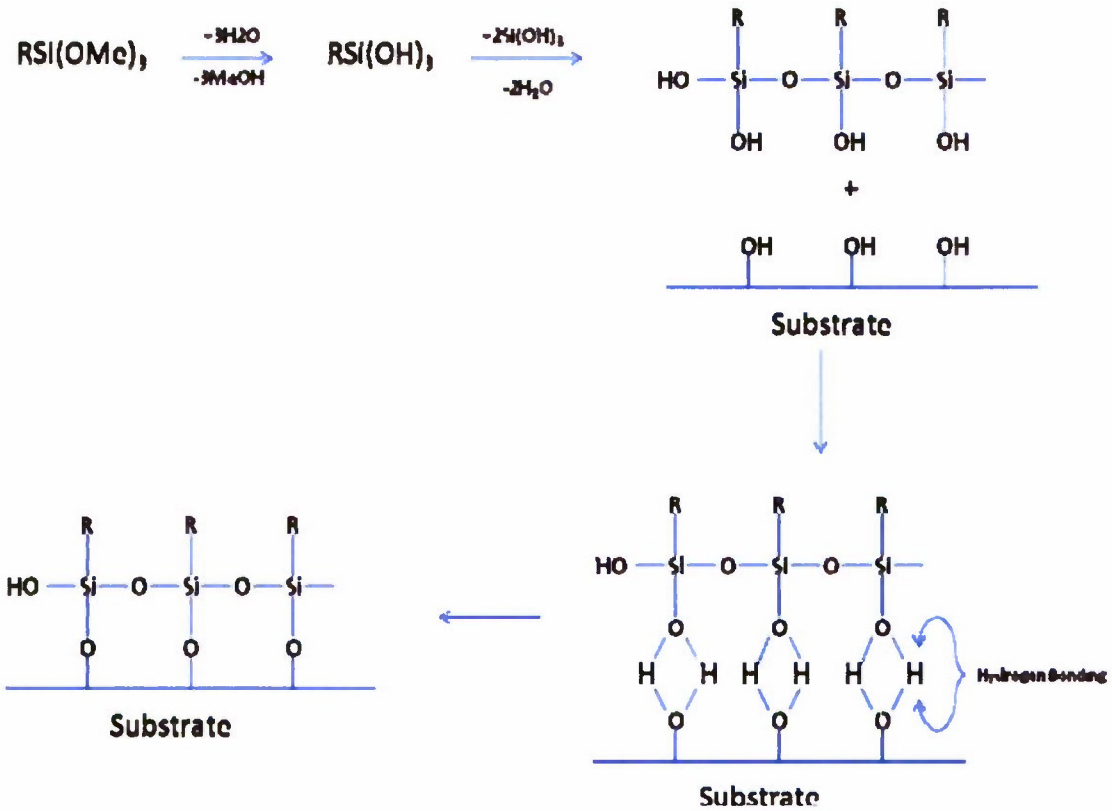

Figure 3 - Reaction of Organosilane with Substrate Particle

Surface modification experiments using organosilanes were performed to determine the impact of coating on the attenuation performance of TiO_2 powder. Four different organosilanes were chosen as coupling agents. These included n-octyltriethyoxysilane (OTES), n-octadecyltrimethoxysilane (OTMS), tridecafluoro-1,1,2,2-tetrahydroctyltrimethoxysilane (TDFTMS), and diphenyldimethoxysilane (DPDMS) (Gelest, Morrisville, PA). Coating was achieved using a Gemco slant-cone blender (0.5 ft^3 working capacity) equipped with an airless liquid injection system and agitator (Gemco, Middlesex, NJ). The liquid injection system was used to introduce the dissolved silane during blending. Millennium TiO_2, grade RCL-9, was

used as the substrate for all coating experiments. RCL-9 was chosen for its high purity and absence of organic coating. A summary of experimental procedures is provided herein:

1. Placed approximately 96 g of a given silane in 125 mL ethanol and magnetically stirred until dissolved.
2. Placed approximately 11.5 kg TiO_2 powder in slant-cone blender and sealed.
3. Preheated the blender to 110 °F, set rotation speed to 4 RPM, and set pressure to 5 in Hg for 5 min.
4. Vessel pressure was subsequently set to 7 in Hg, rotation speed to 22 RPM, and agitator to 3300 ft/min.
5. The silane/ethanol solution was subsequently sprayed in over a 5–7 min period. Rotation and agitation continued during sample introduction.
6. Upon completion of sample introduction, rotation and agitation continued for 5 min.
7. The agitator was turned off.
8. The jacket temperature was set to 105 °C, the rotation speed was decreased to 4 RPM, and the pressure was set to approximately 28 in Hg.
9. Continued blending for approximately 1.5 hr.
10. Cooled batch to ambient temperature and immediately placed coated batch in seal tight containers.

In addition to the experiments involving the hydrophobic organosilanes, two additional coatings that imparted a degree of hydrophilicity were explored. These included trimethylolethane (TME) and trimethylolpropane (TMP). TME and TMP are organic polyols, which are commonly used in the surface modification of pigments. The presence of the three hydroxyl groups allows both TME and TMP to covalently bond to the substrate particle via condensation and curing. Upon completion of bonding, the presence of the free hydroxyl groups imparts a degree of hydrophilicity to the particle surface, which is in contrast to the more hydrophobic organosilane coatings.

Surface modification experiments with TME and TMP were identical to the organosilane experiment with one exception. 0.5% by mass TME or TMP was added rather than the 0.8% used with the organosilanes. This was achieved by dissolving approximately 60 g of TMP or TMP in 100 mL H_2O. All other coating and blending procedures were the same as previous experiments. Proposed mechanisms for the surface modification of a particle with TMP are provided in Figures 4 and 5.

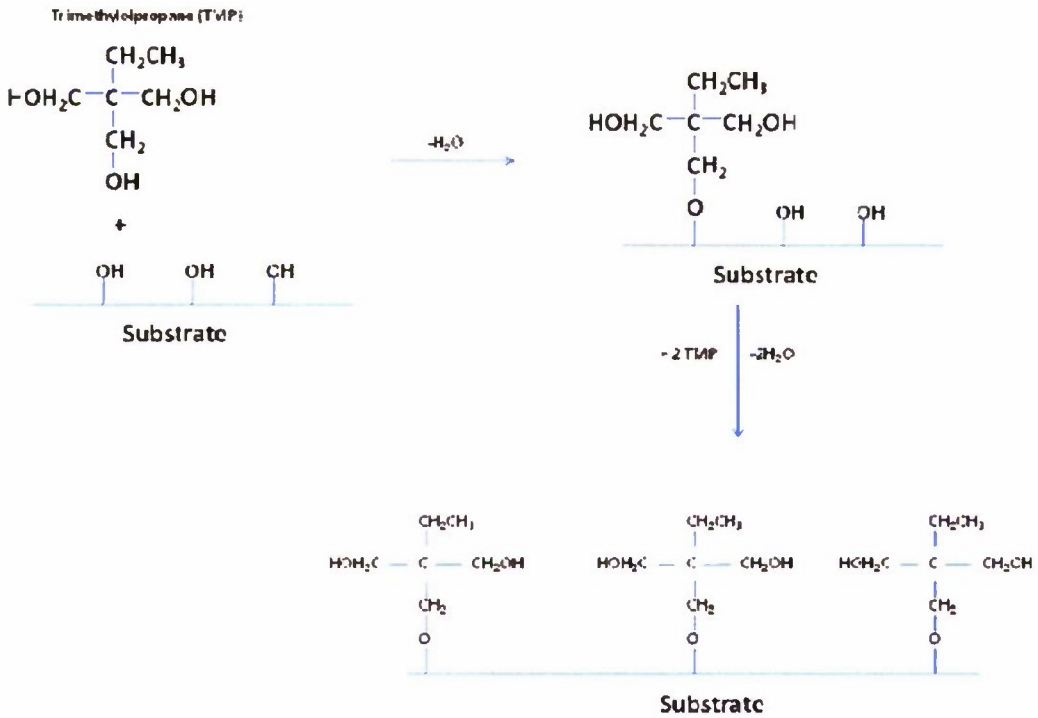

Figure 4 - Proposed Mechanism for the Surface Modification of a Substrate with TMP

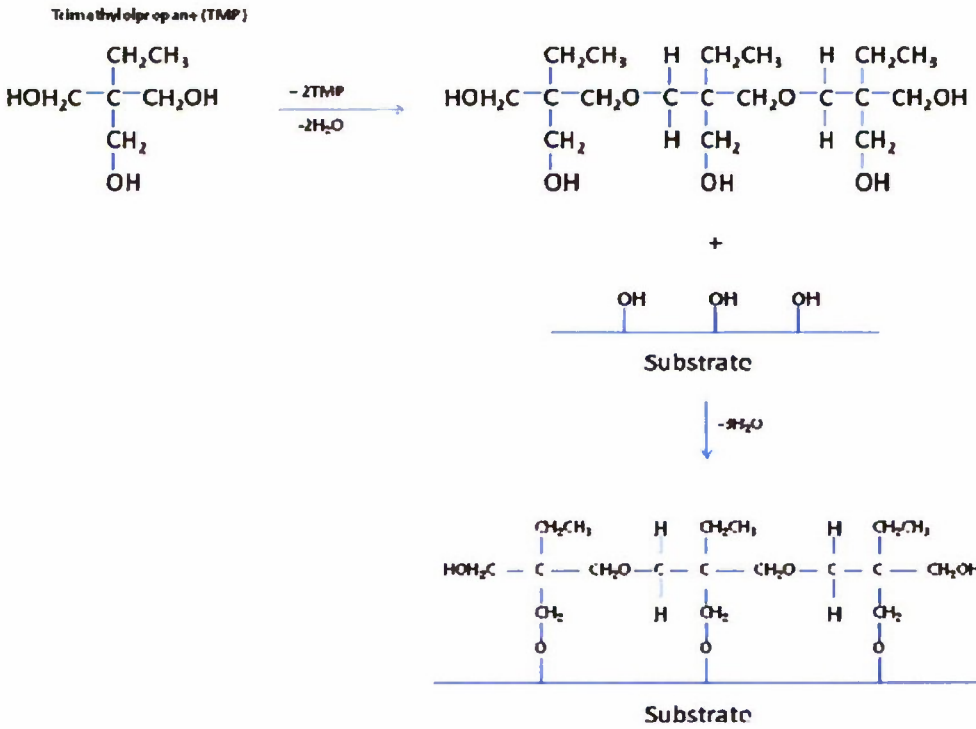

Figure 5 - Alternative Mechanism for the Addition of TMP to a Substrate Particle

Chamber Tests–Pneumatic and Explosive Dissemination of Surface Modified TiO_2

Pneumatic and explosive dissemination of the surface modified powders was achieved in the same manner in which the commercial lots of TiO_2 were disseminated. Namely, the powders were disseminated through an SRI nozzle with an outlet pressure of 90 psi and with a M106 grenade. All powders were tested in triplicate. Mass extinction, yield, and calculated particle diameters were calculated using the methods described in Section II. The pneumatic and explosive results are displayed in Tables 4 and 5, respectively. A comparison of spectra between the uncoated and top performing coated (diphenyldimethoxysilane) versions of lot RCL-9 is also provided in Figure 6.

Table 4 - Pneumatic Dissemination of Surface Modified TiO_2

Material	Extinction (0.4-0.7 μm)	SD	Yield	Calculated Particle Size (μm)
TME Coated TiO_2	3.85	0.39	0.93	2.3
TMP Coated TiO_2	3.77	0.50	0.93	2.6
TDFTMS Coated TiO_2	3.58	0.13	0.93	2.0
DPDMS Coated TiO_2	4.07	0.02	0.96	2.7
n-ODTMS Coated TiO_2	3.83	0.31	0.90	2.2
n-OTES Coated TiO_2	3.76	0.09	0.96	2.2

TME = Trimethylolethane, TMP = Trimethylolpropane, TDFTMS = Tridecafluoro-1,1,2,2-tetrahydroctyltrimethoxysilane, DPDMS = Diphenyldimethoxysilane, n-ODTMS = n-octadecyltrimethoxysilane, n-OTES = n-octyltriethoxysilane.

Table 5 - Explosive Dissemination of Surface Modified TiO_2

Material	Extinction (0.4-0.7 μm)	SD	Yield	Calculated Particle Size (μm)	Fill Fraction	Figure of Merit
TME Coated TiO_2	2.05	0.10	0.24	6.3	0.32	0.67
TMP Coated TiO_2	1.99	0.10	0.24	6.4	0.30	0.61
TDFTMS Coated TiO_2	1.74	0.032	0.22	7.1	0.29	0.47
DPDMS Coated TiO_2	2.46	0.06	0.30	5.4	0.30	0.94
n-ODTMS Coated TiO_2	1.66	0.02	0.18	8.2	0.30	0.38
n-OTES Coated TiO_2	2.08	0.18	0.20	6.4	0.30	0.53

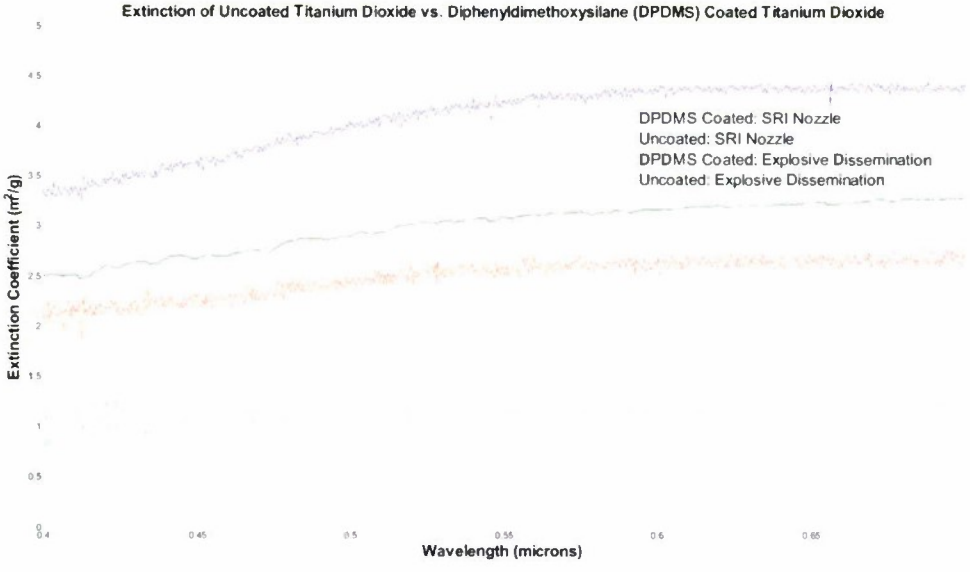

Figure 6 - Extinction Comparison of Uncoated vs. Coated TiO_2

6. MATERIAL CHARACTERIZATION OF TIO_2 POWDERS

Characterization results for all powders are provided herein. The techniques used to characterize the powders include particle size analysis, powder flow measurements, contact angle measurements, SEM, and mass spectrometry. A description of each instrument is also provided. The goal of these tests was to provide a library of information regarding surface modified TiO_2 powders. An additional goal was to determine if any correlation between the physical and obscuration properties of these powders existed.

6.1 Particle Size Analysis

The particle sizes of all powders were measured using a Sympatec (Clausthal-Zellerfeld, Germany) HELOS laser diffraction sensor with a RODOS powder dispersing unit. The instrument houses a HeNe laser (632.8 nm) and Fourier lens. Upon introduction of the particles into the beam, the beam is diffracted at an angle θ that is indicative of the particle size. The diffracted beam is focused by the Fourier lens onto a multi-element photo detector containing 31 semi-circular rings. The intensity and spatial distribution of the diffracted light on the 31 semi-circular detector rings is used as a basis for determining particle size and distribution. Particle size results for the commercial and experimentally coated powders are provided in Tables 6 and 7.

Table 6 - Particle Size of Commercial TiO_2 Powders

Material	Bulk Powder Particle Size (μm)
Tiona 188	1.21
Tiona 595	0.9
Tiona 596	1.7
Tiona RCL-4	1.6
Tiona RCL-9	1.6
R101	3.3
R700	1.0
R706	1.3
R900	1.6
R931 W26	1.1
CR-470	0.9
CR-813	1.3
CR-826	1.1
CR-834	1.5

Table 7 - Particle Size of Experimentally Coated TiO_2 Powders

Material	Bulk Powder Particle Size (μm)
TME Coated TiO_2	3.4
TMP Coated TiO_2	1.6
TDFTMS Coated TiO_2	3.0
DPDMS Coated TiO_2	0.7
n-ODTMS Coated TiO_2	0.7
n-OTES Coated TiO_2	2.3

6.2 Powder Flow Characteristics

The flow properties of all powders were tested with a Hosokawa PT-S powder tester. The instrument provides a means by which eight powder measurements and two calculations may be determined as per the ASTM test designation D6393-08.[7] These ten measurements make up the Carr Indices, which encompass a series of tests used to characterize bulk solids.

The goal of the testing was to determine if there were one or more powder measurements that correlated with chamber results, i.e., aerosol extinction. Test results for the commercial powders are provided in Tables 10–11. Test results for the experimentally coated powders are provided in Tables 13–14. Brief definitions of each Carr Index test are provided herein.

Carr Angle of Repose - a measurement from the powder heap built up by dropping the material through a vibrating sieve and funnel above a horizontal plate.
Carr Angle of Fall - an angle of repose measured from a powder heap to which a defined impulse shock has been applied three times.
Carr Angle of Difference - the difference between the Carr Angle of Repose and Carr Angle of Fall.
Carr Loose Bulk Density, L - a measurement obtained by sieving the sample through a vibrating chute to fill a measuring cup with a volume 100 cm^3. The mass of powder in the cup is measured after the material is flush with the top of the cup.
Carr Packed Bulk Density, P - a measurement obtained by dropping a measuring cup, which is filled with the sample, a specific number of times from the same height for a period of 180 seconds. This is also known as Tapped Bulk Density. The mass of powder in the 100 cm^3 measuring cup is measured after the material is flush with the top of the cup.
Carr Compressibility, C - a calculation related to the Carr Loose Bulk Density and Carr packed Bulk Density values via eq 23:

$$Compressibility = \left(\frac{P-L}{P}\right)\times 100 \tag{23}$$

Carr Dynamic Bulk Density, W (eq 24):

$$W = \left[\left(\frac{P-L}{C}\right)\times 100\right] + L \tag{24}$$

Carr Cohesion - a descriptive measure of interparticle forces based on the rate at which particles pass through sieves. The measurement is performed by placing approximately 2.0 g of material on top of three stacked sieves. The top sieve has the largest opening, the middle sieve has intermediate sized openings, and the bottom sieve has the smallest openings. The sieves are placed and fastened to a vibration plate. The vibration is set to an amplitude of 1.0 mm. The vibration time is based on the Carr Dynamic Bulk Density, the Carr Compressibility, the Carr Loose Bulk Density, and the Carr Packed Bulk Density. The masses retained on each sieve after vibration is complete are used to calculate the Carr Cohesion.
Carr Angle of Spatula - a measurement from the powder heap formed on a spatula that had been buried and then extracted from a bed of powder.
Carr Dispersibility - a measurement by which a powder sample is dropped through a hollow cylinder above a watch glass and then the amount of powder collected by the watch glass is measured.
Flowability - a composite index of angle of repose, compressibility, angle of spatula, uniformity, and cohesion describing the flow properties of a given powder (see Table 8).[8]

Table 8 - Carr Indices Chart of Flowability

Degree of Flowability	Flowability Index
Very Good	90-100
Fairly Good	80-89
Good	70-79
Normal	60-69
Not Good	40-59
Bad	20-39
Very Bad	0-9

Floodability - a composite index of flowability, angle of fall, angle of difference, and dispersibility describing the powders' ability to flow as a liquid due to the aeration of a mass of particles by air (see Table 9).[8]

Table 9 - Carr Indices Chart of Floodability

Degree of Floodability	Floodability Index
Very High	80-100
Fairly High	60-79
Tends to Flush	40-59
May Flush	25-39
Won't Flush	0-24

In addition to the Carr Index results, correlation coefficients, r_{xy}, between the individual Carr Indices and the extinction coefficient were calculated using eq 25:

$$r_{xy} = \frac{\sum_{i=1}^{n}(x_i-\bar{x})(y_i-\bar{y})}{(n-1)s_x s_y} \tag{25}$$

Where n is the number of measurements, x is the extinction variable, y is the individual Carr index measurement, s_x is the standard deviation of the extinction measurement, and s_y is the standard deviation of the Carr index measurement. The correlation coefficient equals 0 if the two variables are independent, 1 in the case of an increasing linear relationship, -1 in the case of a decreasing linear relationship, or somewhere in between. The closer the coefficient is to 1 or -1, the stronger the correlation there is between the two variables. The correlation coefficient results for the commercial and experimental powders are provided in Tables 12 and 15.

Table 10 - Floodability Test Results for Commercial TiO_2 Powders

Material	Angle of Fall (degrees)	Angle of Difference (degrees)	Dispersibility (%)	Total Floodability Index
Tiona 188	36.5	7	20.6	37
Tiona 595	25.1	17.3	26.5	53
Tiona 596	23.6	20.6	26.5	56
Tiona RCL-4	30.5	10.2	17	39
Tiona RCL-9	23.3	20.9	14	51
R101	24.4	18.0	18.0	56
R700	25.4	17.3	19	15
R706	28.8	13.8	24.8	16
R931 W26	22.1	19.3	14.7	12
CR-470	30.2	15.9	23.1	56
CR-813	25.9	17.1	14.8	12
CR-826	36.2	6	59	25
CR-834	31.4	12.2	26	45

Table 11 - Flowability Results for Commercial TiO_2 Powders

Material	Angle of Repose (degrees)	Aerated Bulk Density (g/cm^3)	Packed Bulk Density (g/cm^3)	Compressibility (%)	Average Angle of Spatula (degrees)	Cohesion (%)	Flowability Index
Tiona 188	43.5	0.859	1.228	30	54.5	95.5	44
Tiona 595	42.4	0.895	1.286	30.4	54.8	87.8	44
Tiona 596	44.2	0.694	1.124	38.3	53.6	74.8	39
Tiona RCL-4	40.7	0.867	1.342	35.4	55.7	87.3	40
Tiona RCL-9	44.2	0.664	1.162	42.9	56.7	68.6	36
R101	42.4	0.672	0.947	29	57.5	62.6	46
R700	42.7	0.73	1.235	40.9	59.8	92.1	33
R706	42.6	0.797	1.256	36.5	53.2	93.9	37
R931-W26	41.4	0.432	0.715	39.6	52.6	60.7	37
CR-470	46.1	0.911	1.313	30.6	55.6	88.4	28
CR-813	43	0.443	0.764	42	48.4	26.3	46
CR-826	42.2	0.735	1.101	33.2	59.8	75.5	40
CR-834	43.6	0.791	1.085	27.1	56.3	70.1	46

Table 12 - Commercially Available Powders-Correlation Coefficients for Extinction vs. Powder Characteristic

Powder Characteristic	SRI Dissemination	Explosive Dissemination
Angle of Fall	0.17	0.62
Angle of Difference	-0.13	-0.57
Dispersibility	-0.30	0.57
Floodability Index	-0.31	-0.31
Angle of Repose	0.18	0.15
Aerated Bulk Density	0.60	0.67
Packed Bulk Density	0.65	0.52
Compressibility	-0.11	-0.63
Average Angle of Spatula	-0.06	0.43
Cohesion	0.66	0.62
Flowability Index	-0.10	0.16

Table 13 - Floodability Results for Experimentally Coated TiO_2 Powders

Material	Angle of Fall (degrees)	Angle of Difference (degrees)	Dispersibility (%)	Total Floodability Index
TME Coated TiO_2	27	16.3	8.7	43.5
TMP Coated TiO_2	22.2	22.4	30.2	57.0
TDFTMS Coated TiO_2	25.3	18.4	19.8	52.0
DPDMS Coated TiO_2	22.4	23.1	36.8	61.5
n-ODTMS Coated TiO_2	20.7	24.5	4.9	46.0
n-OTES Coated TiO_2	24.7	17.6	27.1	54.0

Table 14 - Flowability Results for Experimentally Coated TiO_2 Powders

Material	Angle of Repose	Aerated Bulk Density (g/cm^3)	Packed Bulk Density (g/cm^3)	Compressibility (%)	Average Angle of Spatula (degrees)	Cohesion (%)	Flowability Index
TME Coated TiO_2	43.3	0.699	1.35	48.2	60.7	93.6	30.5
TMP Coated TiO_2	44.6	0.672	1.281	47.5	57.9	94.7	31
TDFTMS Coated TiO_2	43.7	.652	1.244	47.6	52.5	81.9	32
DPDMS Coated TiO_2	45.5	0.667	1.313	49.2	63.4	95.4	26.5
n-ODTMS Coated TiO_2	45.2	0.625	1.271	50.8	62.6	77.5	29
n-OTES Coated TiO_2	42.3	0.671	1.288	47.9	49.6	93.7	32

Figure 15 - Experimentally Coated Powders-Correlation Coefficients between Extinction and Powder Characteristic

Powder Characteristic	SRI Dissemination	Explosive Dissemination
Angle of Fall	-0.34	0.08
Angle of Difference	0.43	-0.02
Dispersibility	0.29	0.72
Floodability Index	0.32	0.64
Angle of Repose	0.53	0.11
Aerated Bulk Density	0.18	0.57
Packed Bulk Density	0.65	0.62
Compressibility	0.49	-0.15
Average Angle of Spatula	0.73	0.23
Cohesion	0.45	0.84
Flowability Index	-0.89	-0.53

6.3 Contact Angle Measurements

Contact angle measurements were determined for all powders using a Future Digital Scientific Corporation (Garden City, NY) OCA 15 device. Contact angle is the measurement at which a given liquid meets the solid surface. Typically, the contact angle of a water droplet is used on a solid surface that is flat. In these tests, to produce a flat solid surface of the TiO_2 powders, the powders were pressed into a pellet, and a liquid droplet was subsequently dispensed onto the surface of the pellet. Contact angle provides a measure of hydrophobocity. A liquid water droplet will, for example, spread onto a hydrophilic surface and the contact angle will be minimal. Conversely, if the solid surface is hydrophobic, the contact angle will be in the range of 90 to 150°. The goal of this study was to determine if there was any correlation between extinction and contact angle. The contact angles for the commercial and experimentally coated powders are provided in Tables 16 and 17. Correlation coefficients between contact angle and extinction were calculated for the commercial and experimental powders. In the analysis of commercial powders, correlation coefficients of 0.80 and 0.47 were observed for the SRI and explosive disseminations, respectively. In the analysis of the experimental powders, correlation coefficients of 0.11 and -0.02 were observed for the SRI and explosive disseminations, respectively.

Table 16 - Contact Angle Measurements of Commercially Available Powders

Material	Contact Angle (Degrees)	Comment
Tiona 188	143.5	Static
Tiona 595	88.0	Dynamic
Tiona 596	78.6	Dynamic
RCL-4	146.0	Static
RCL-9	66.7	Dynamic
R101	30.0	Dynamic
R700	94.0	Dynamic
R706	80.1	Dynamic
R931-W26	76.0	Dynamic
CR-470	152.0	Static
CR-813	57.3	Dynamic
CR-826	64.2	Dynamic
CR-834	45.5	Dynamic

Table 17 - Contact Angle Measurements of Experimentally Coated TiO_2

Material	Contact Angle (Degrees)	Comment
DPDMS Coating	137.2	Static
n-OTES Coating	151.5	Static
n-ODTMS	147.1	Static
TDFTMS	119.8	Dynamic
TME	66.8	Dynamic
TMP	72.9	Dynamic

6.4 SEM

TiO_2 powders were analyzed for particle shape, granule size, and extent of agglomeration using a JEOL JCM-5700 Scanning Electron Microscope. Images of the highest performing commercial lot, CR-470, and the highest performing experimental coating, diphenyldimethoxysilane, are provided in Figures 7–11.

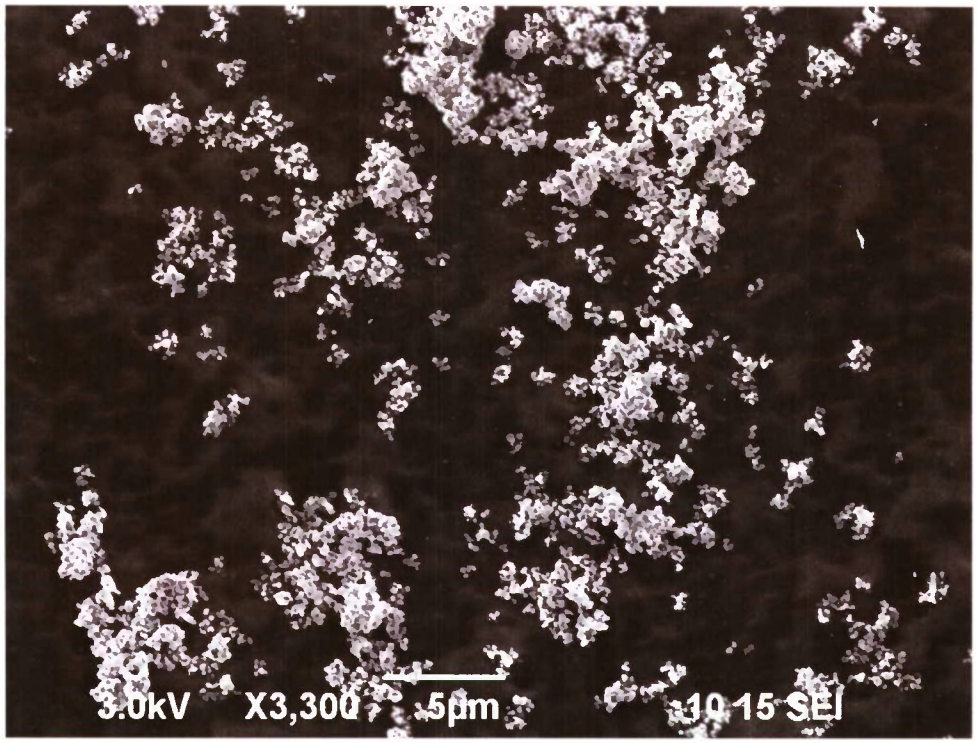

Figure 7 - SEM Image #1 of CR-470

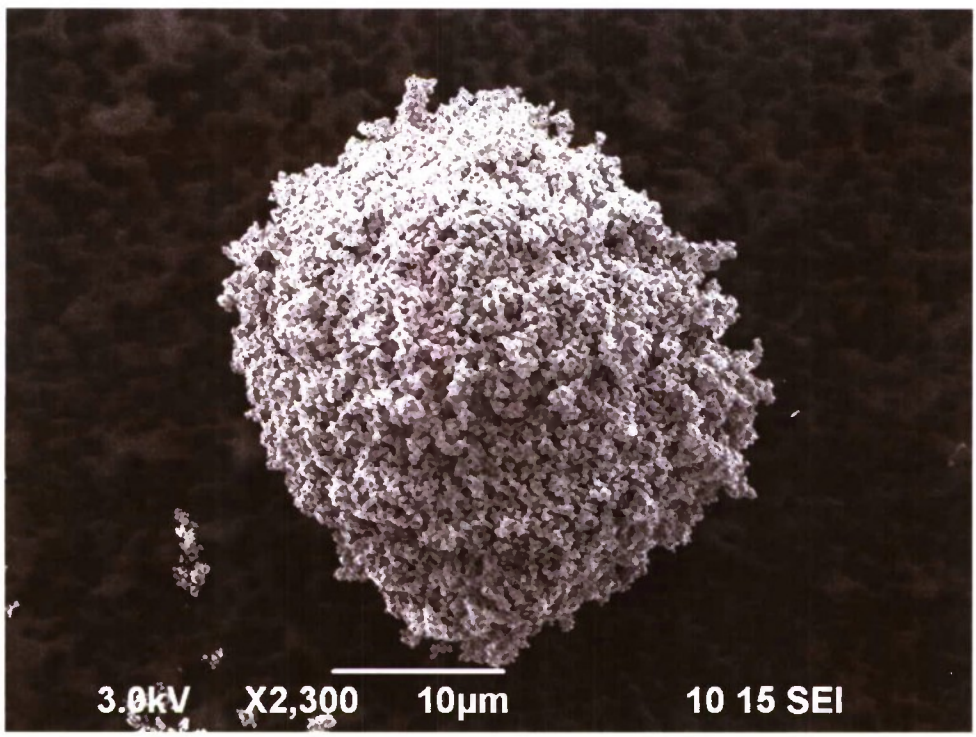

Figure 8 - SEM Image #2 of CR-470

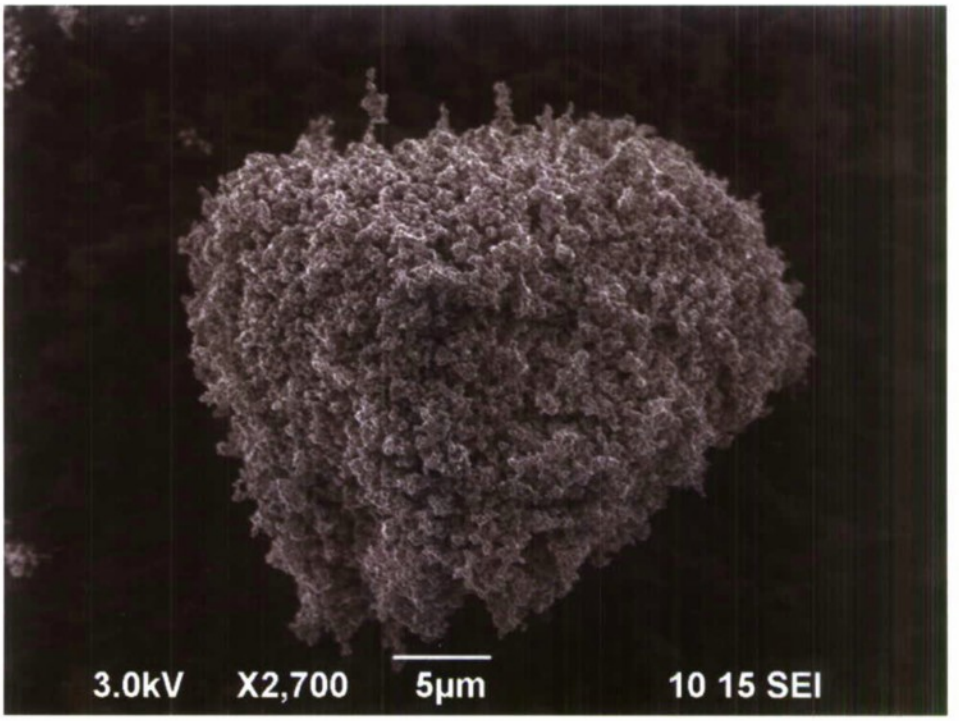

Figure 9 - SEM Image #1 of Diphenyldimethoxysilane Coated TiO_2

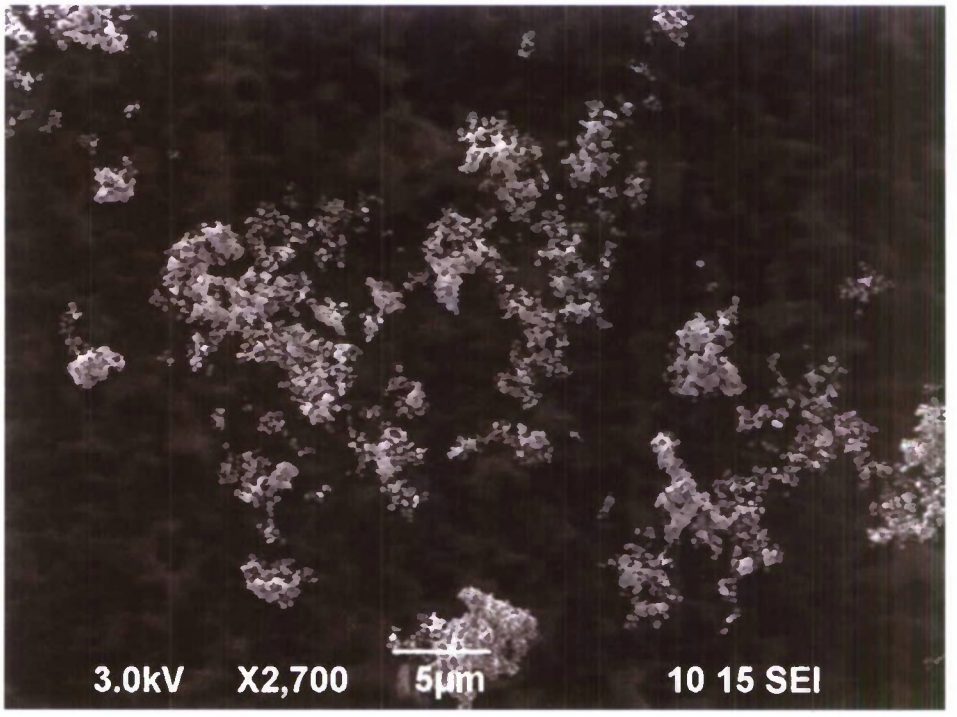

Figure 10 - SEM Image #2 of Diphenyldimethoxysilane Coated TiO_2

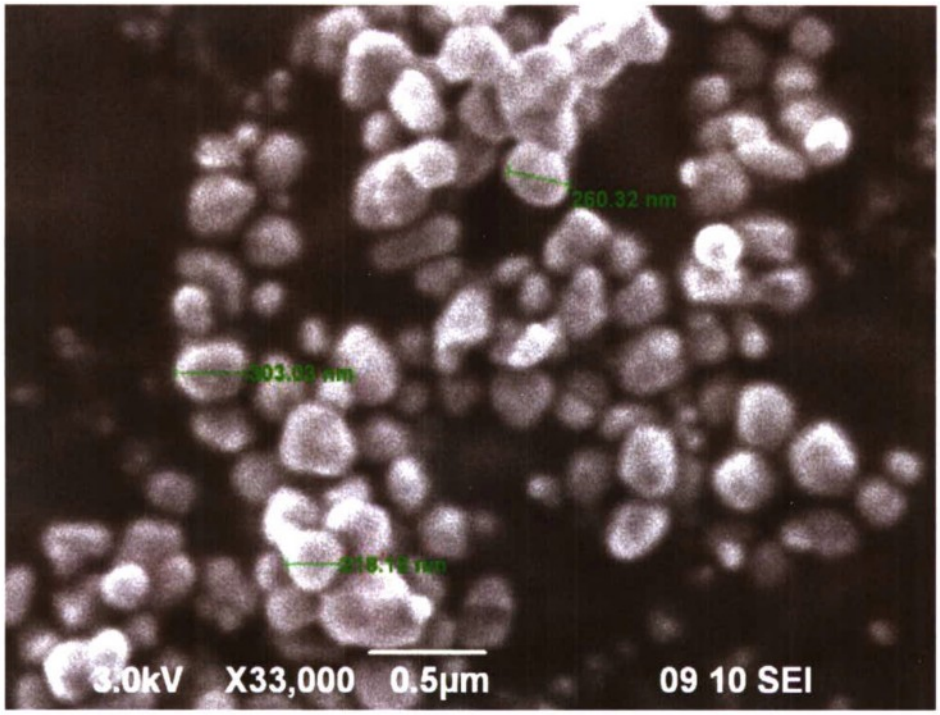

Figure 11 - SEM Image #3 of Diphenyldimethoxysilane Coated TiO_2

6.5 Mass Spectrometry Analysis

Mass spectrometry was used to elucidate the chemical content of the coatings used in two of the higher performing commercial powders. These two lots included Tronox CR-470 and Tronox CRX. Tronox CRX is an experimental lot of TiO_2 manufactured by Kerr-McGee in the early 1990s. This particular lot, dubbed the "magic barrel" lot, historically produced one of the highest figure of merit values observed in the ECBC smokes chamber. Due to insufficient quantities, this particular lot was not included in this particular report for chamber analysis and powder characterization. However, a sufficient amount was available for analysis via mass spectrometry.

Mass spectrometry experiments involved the use of a JEOL (Dearborn, MA) AccuTOF-DART mass spectrometer. This instrument is equipped with a direct analysis in real time (DART) atmospheric pressure ion source that ionizes gases, liquids, and solids in open air at ambient conditions. Sample preparation involved placing the TiO_2 in 2 mm OD Pyrex melting point tube. The tube was cleaned in the DART gas stream (Helium) prior to sampling in order to remove any residual dioctyl adipate plasticizer.

MS Conditions:

DART Gas Heater Temp:	350 °C
Glow Discharge Needle:	3500V
Intermediate Electrode:	+150V
Grid Electrode:	+250V
MS RF Ion Guide:	600V

Blown up images of the most abundant peaks observed for Tronox CR-470 are provided in Figures 12–14.

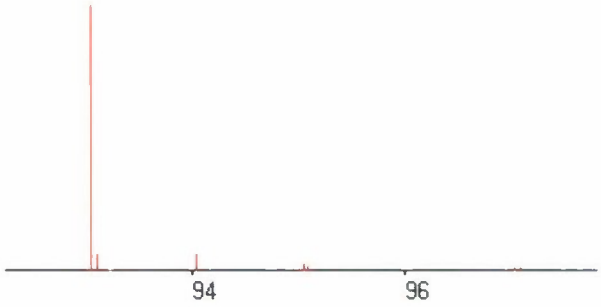

Figure 12 - Tronox CR-470 Mass Spectra, m/z 93 Peak

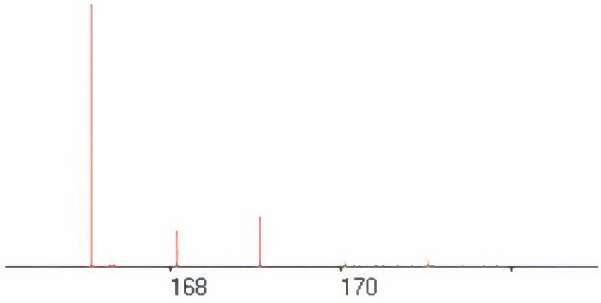

Figure 13 - Tronox CR-470 Mass Spectra, m/z 167 Peak

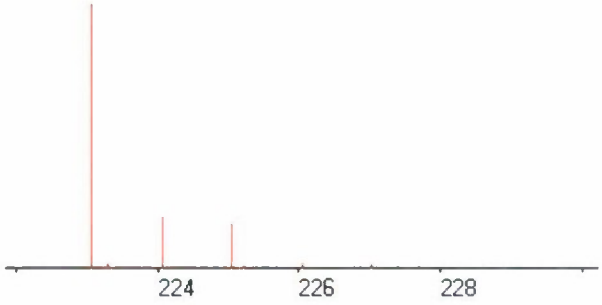

Figure 14 - Tronox CR-470 Mass Spectra, m/z 223 Peak

Peaks at m/z 93, 167, and 223 were observed for lot CR-470. A proposed structure for the coating used in lot CR-470 is dimethyldihydroxysilane, which has a molecular weight of 92 amu. The structure of dimethyldihydroxysilane is provided in Figure 15. This identification is consistent with the [M+H] peak observed at 93 amu (m/z 93). The identification is also consistent with condensation reactions which form dimers (m/z 167) and ring structured trimers (m/z 223). The proposed structures for the dimer and trimer are provided in Figures 16 and 17.

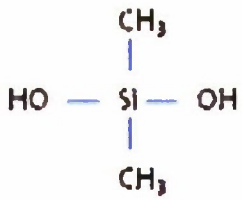

MW = 92 amu

Figure 15 - Proposed Structure for the Coating Used in Tronox CR-470

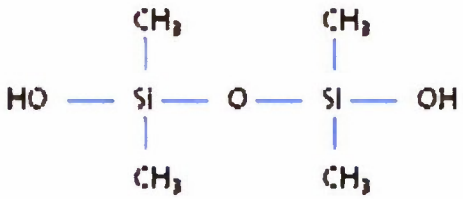

MW = 166 amu

Figure 16 - Proposed Structure for the Dimer Form of the Coating Used in CR-470

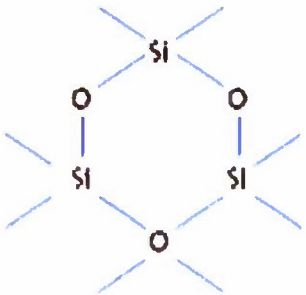

MW = 222 amu

Figure 17 - Proposed Structure for the Trimer Form of the Coating Used in CR-470

Mass spectrums observed for the CRX lot are provided in Figures 18–19.

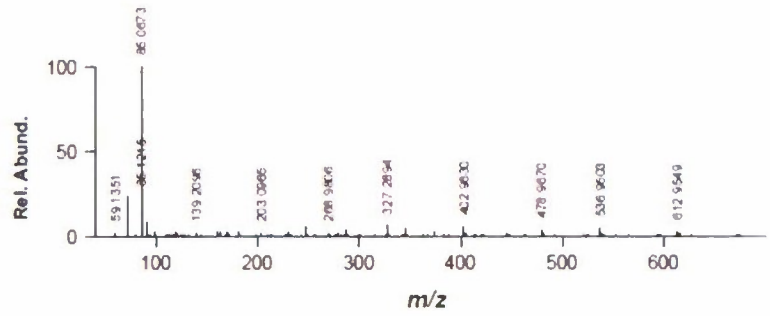

Figure 18 - Mass Spectrum for Lot CRX (range = m/z 0-700)

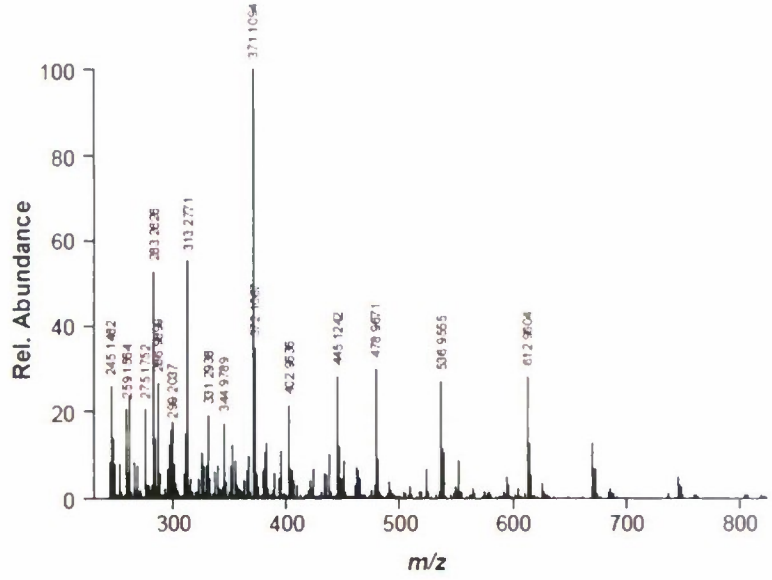

Figure 19 - Mass Spectrum of Lot CRX (range = m/z 220-820)

The most abundant peak observed in Figure 18 occurred at m/z 85. Software analysis provided an exact mass calculation of 85.0673 amu with a molecular formula of C_5H_9OSi. The most abundant peak observed in Figure 19 occurred at m/z 371. Common fragments with differences of 58 amu (671-613, 537-479, 371-313), 74 amu (747-671, 445-371), and 76 amu (613-537, 479-403) were also observed in this spectrum. This repetitive fragmentation pattern is indicative of the presence of an oligomer. Proposed structures for the 58, 74, and 76 amu are provided in Figure 20. Additionally, a proposed structure for the peak at m/z 371 is provided in Figure 21. These proposed structures are consistent with the fragmentation patterns and masses observed in Figures 20 and 21.

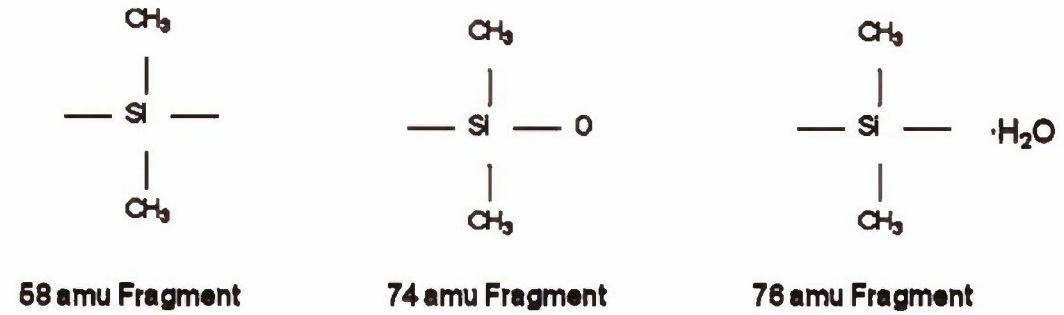

Figure 20 - Proposed Structures for 58, 74, and 76 amu Fragments Observed in Lot CRX

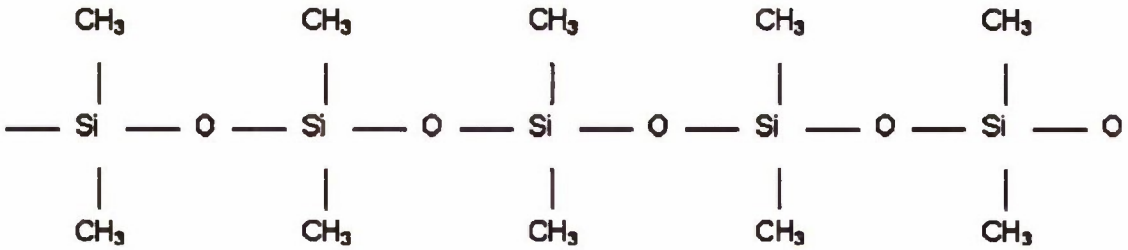

Figure 21 - Proposed Structure for 371 amu Fragment Observed in Lot CRX

The structures proposed in Figures 20 and 21 indicate that the coating used in the CRX lot is an organosilane. More specifically, the organosilane is a dialkyl or dimethylsilane. However, the fragmentation patterns do not definitively reveal the identity of the two hydrolyzable groups that are present. The presence of two hydrolyzable groups is assumed due to the formation of the oligomeric structure proposed in Figure 21. Due to insufficient evidence, the proposed structure for the coating used in the CRX lot is provided in Figure 22. Here X corresponds to a generic hydrolyzable group. Further studies using alternative surface analysis such as non-dispersive infrared (NDIR), X-ray photoelectron spectroscopy (XPS), or NMR are required to definitively identify the hydrolyzable groups used in lot CRX.

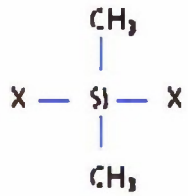

Figure 22 - Proposed Structure for the Coating Used in Lot CRX

7. CONCLUSIONS

The grenade figure of merit was the primary metric by which all TiO_2 powders were judged. Among the commercially tested grades of TiO_2 powders, Tronox CR-470 exhibited the highest figure of merit at 0.63. This was significantly higher than any other commercial powder that was tested. The relatively large extinction, fill fraction, and yield observed for CR-470 contributed to its superior performance.

When comparing dissemination techniques, pneumatic dissemination clearly produces higher extinction values and yield than explosive dissemination. This observation is supported by the fact that the calculated particle sizes for the pneumatically disseminated powders are significantly smaller than the explosively disseminated powders, as demonstrated in Tables 2 and 3. Hence, it is concluded that explosive dissemination produces particle agglomeration and an increase in particle size.

Superior performance during pneumatic dissemination did not necessarily result in superior performance during explosive dissemination. For example, Tiona 188 exhibited the highest extinction during pneumatic dissemination but had a figure of merit of almost half that of Tronox CR-470 when explosively disseminated. It is hypothesized that the coating used in a given lot plays a significant role in agglomeration during the explosive dissemination process.

Surface modification experiments using the Gemco slanted cone blender yielded superior results, relative to those obtained for the commercial powders. Certain coatings using this technique resulted in higher figures of merit than the highest performing commercial material. For example, the diphenyldimethoxysilane (DPDMS) coated material exhibited a figure of merit of 0.94, which represents a 49% improvement over Tronox CR-470. It was also observed that this dialkyl organosilane coating produced a higher figure of merit than the monoalkyl organosilane coatings. Clearly, the chosen coating and/or coating process impacts on figure of merit.

Also of note is the fact that the highest performing TiO_2 powders in both the commercial powder class and the experimentally coated class were coated with dialkylsilanes. The highest performing experimental coating, DPDMS, contains the diphenyl functionality while the coating used in the highest performing commercial lot, CR-470, contains the dimethyl functionality. Additionally, it was concluded from mass spectrometry analysis that the historically high performing CRX lot also contains the dimethyl functionality. A dialkyl organosilane intrisically contains two hydrolyzable groups. These two groups serve as sites for both polymerization reactions with other like silanes and for condensation reactions with particle surfaces.

With regard to the Carr index measurements, significant correlations (near 1 or -1) between mass extinction and a given flow property were not observed. Moderate correlations (|0.5 to 0.7|) for the explosively disseminated commercial powders were observed for angle of fall, angle of difference, dispersibility, aerated bulk density, packed bulk density, compressibility, and cohesion. Likewise, moderate correlations (|0.5 to 0.8|) for the explosively disseminated experimentally coated powders were observed for dispersibility, floodability, aerated bulk

density, packed bulk density, and cohesion. Although these indices may be used as descriptive characteristics of the powders, results did not indicate that they may be used as definitive tools for predicting the mass extinction coefficient.

Similarly, contact angle results did not yield significant correlations between mass extinction and contact angle. However, as demonstrated by the experimentally coated materials, contact angle measurements may be used to predict whether or not a given powder was sufficiently coated with a hydrophobic or hydrophilic coating. For example, all of the hydrophobic organosilanes (DPDMS, n-OTES, nODTMS, and TDFTMS) exhibited contact angles of 120° or greater. Likewise, the hydrophilic TME and TMP coatings yielded contact angles that were less than 73°. Hence, contact angle measurement may not be used as a tool for predicting mass extinction, but can be used to predict whether or not given coating or coating technique sufficiently produced a hydrophobic or hydrophilic powder.

8. RECOMMENDATIONS

Future studies should focus on the exploration of a wide range of dialkyl organosilane coatings, and subsequently trialkyl organosilanes. Additionally, commercial coating processes should be thoroughly explored and compared with the Gemco slanted-cone blending technique used in this study. Theoretical mass extinction calculations, as exemplified in Figure 1, indicate that there is significant room for improvement in the extinction values of titanium dioxide (TiO_2) powders. This can be achieved in a large part by producing the optimum mean particle diameter of ~0.20 μm post dissemination. Coatings have a significant impact on surface energy, the prevention of agglomeration, and particle size. Therefore, optimization of the TiO_2 coating process is one way in which the figure of merit for the M106 grenades may be improved.

LITERATURE CITED

1. Winkler, J. *Titanium Dioxide*; Vincentz Network: Hanover, Germany, 2003.

2. Embury, J.F. *Optical Engineering* **1983**, *22*(1), 71-77.

3. Bohren, C.F.; Huffman, D.R. *Absorption and Scattering of Light by Small Particles*; Wiley-VCH: Weinheim, Germany, 2004 .

4. Hinds, W.C. *Aerosol Technology: Properties, Behavior, and Measurement of Airborne Particles*; John Wiley & Sons: New York, 1999.

5. Lowe, R.L. *Engineering Development of Grenade, Launcher, Smoke: IR Screening M76*; CRDEC-CR-012; U.S. Army Chemical Research, Development and Engineering Center: Aberdeen Proving Ground, MD, 1988; UNCLASSIFIED Report (AD B131 223).

6. Arkles, B. *Kirk-Othmer Encyclopedia of Chemical Technology*; 4th ed.; vol. 22; John Wiley & Sons: New York, 1997, 69-81.

7. ASTM D6393-08, *Standard Test Method for Bulk Solids Characterization by Carr Indices*, ASTM International.

8. Carr, R.L. *Chemical Engineering* **1965**, *18*(1), 163-168.

Blank

APPENDIX

MATLAB CODE

Mie_lambda_scan.m - Computation of Mass Extinction Coefficients

```
% Computation of Mass Extinction Coefficients for a given relative
% complex refractive index ratio (m=m'+im''), a range of particle sizes,
% and range of incident visible wavelengths. The index of absorption
% ratio, m'', was assumed to equal zero for titanium dioxide in the visible.

% The relative refractive index, m', for titanium dioxide was assumed
% to be 2.74 throughout the visible region.

% Brendan G. DeLacy, May, 2010


function result = Mie_lambda_scan(m)

% Here m is the refractive index ratio. For Titanium Dioxide, m = 2.74.

lambda = (400:1:700); % Incident visible wavelengths in nm.

lambda = lambda'; % Transposes the matrix.

nlambdas = numel(lambda); % Determines the number of elements in the matrix

r = 60:10:120; % The radii of the particles in nanometers

r_m = r.*0.000000001; % The radii if the particles in meters

nr = numel(r); % The number of columns of r, or the number of radii

density = 4.23; % density of titanium dioxide in g/cc


for j = 1:nlambdas

   for k = 1:nr

   x(j,k) = 2*pi*r(1,k)./lambda(j,1);

   Q(j,k) = Mie_Qext(m,x(j,k));
```

```
    C_ext(j,k) = Q(j,k).*r_m(1,k)^2*pi; % r must be in meters

    volume(1,k) = (4/3).*r_m(1,k)^3.*pi*1000000; % volume in cm^3

    alpha_cc(j,k) = C_ext(j,k)./volume(1,k);
    % The volume extinction coefficient

    alpha_g(j,k) = alpha_cc(j,k)./density;
    % The mass extinction coefficient

    end

end


plot(lambda,alpha_g);

title(42print('Mass Extinction Cocfficient (Refractive Indcx = 2.74)'))

xlabel('wavelength (nm)')

ylabel('MEC (m^2/g)')

result = alpha_g;
```

Mie_Qext.m - Computation of the Extinetion Efficieney

```
funetion result = Mie_Qext(m, x)

% Computation of Mie Effieieneies for a given
% eomplex refractive-index ratio m=m'+im"
% and size parameter x=k0*a, where k0= wave number in ambient
% medium, a=sphere radius, using complex Mie Coeffieients
% an and bn for n=1 to nmax.
% Result is the extinetion effieney (qext).
% Uses the funetion "Mie_abed" for an and bn, for n=1 to nmax.

% Code ereated by C. Mätzler, May 2002, Matlab Funetions for Mie
% Seattering and Absorption, Researeh Report No. 2002-08, June, 2002,
% Institut fur Angewandte Physik.

% Referenee: Bohren and Huffman (1983), "Absorption and Scattering of
% Light by Small Partieles, p. 103,119-122,477.



If x==0              % To avoid a singularity at x=0

   result = [real(m) imag(m) 0 0 0 0 0 0 1.5];

elseif x>0           % This is the normal situation

   nmax = round(2+x+4*x.^(1/3));

   n1 = nmax-1;

   n = (1:nmax);en = 2*n+1; e1n = n.*(n+2)./(n+1); c2n = en./n./(n+1);

   x2 = x*x;

   f = mie_abed(m,x);

   anp = (real(f(1,:))); anpp = (imag(f(1,:));

   bnp = (real(f(2,:))); bnpp = (imag(f(2,:));

   g1(1:4,nmax) = [0; 0; 0; 0]; % displaeed numbers used for

   g1(1,1:n1) = anp(2:nmax);    % asymmetry parameter, p. 120
```

```
    g1(2,1:n1) = anpp(2:nmax);
    g1(3,1:n1) = bnp(2:nmax);
    g1(4,1:n1) = bnpp(2:nmax);
    dn = cn.*(anp+bnp);
    q = sum(dn);
    qext = 2*q/x2;
    en = cn.*(anp.*anp+anpp.*anpp+bnp.*bnp+bnpp.*bnpp);
    q = sum(en);
    qsca = 2*q/x2;
    qabs = qext-qsca;
    fn = (f(1,:)-f(2,:)).*cn;
    gn = (-1).^n;
    f(3,:) = fn.*gn;
    q = sum(f(3,:));
    qb = q*q'/x2;
    asy1 = c1n.*(anp.*g1(1,:)+anpp.*g1(2,:)+bnp.*g1(3,:)+bnpp.*g1(4,:));
    asy2 = c2n.*(anp.*bnp+anpp.*bnpp);
    asy = 4/x2*sum(asy1+asy2)/qsca;
    qratio = qb/qsca;
    result =[qext];
end;
```

Mie_abcd.m - Computation of the Mie Scattering Coefficients

```
function result = Mie_abcd(m, x)


% Computes a matrix of Mie coefficients, a_n, b_n, c_n, d_n,
% of orders n=1 to nmax, complex refractive index m=m'+im",
% and size parameter x=k0*a, where k0= wave number
% in the ambient medium, a=sphere radius;

% Code created by C. Mätzler, May 2002, Matlab Functions for Mie Scattering
% and Absorption, Research Report No. 2002-08, June, 2002,
% Institut fur Angewandte Physik.

% Reference: Bohren and Huffman (1983), "Absorption and Scattering of Light by Small
Particles, p. 103,119-122,477.


nmax = round(2+x+4*x.^(1/3));

n = (1:nmax);
nu = (n+0.5);
z = m.*x;
m2 = m.*m;

sqx = sqrt(0.5*pi./x);

sqz = sqrt(0.5*pi./z);

bx = besselj(nu, x).*sqx;

bz = besselj(nu, z).*sqz;

yx = bessely(nu, x).*sqx;

hx = bx+i*yx;

b1x = [sin(x)/x, bx(1:nmax-1)];

b1z = [sin(z)/z, bz(1:nmax-1)];

y1x = [-cos(x)/x, yx(1:nmax-1)];

h1x = b1x+i*y1x;
```

```
ax = x.*b1x-n.*bx;

az = z.*b1z-n.*bz;

ahx= x.*h1x-n.*hx;

an = (m2.*bz.*ax-bx.*az)./(m2.*bz.*ahx-hx.*az);

bn = (bz.*ax-bx.*az)./(bz.*ahx-hx.*az);

cn = (bx.*ahx-hx.*ax)./(bz.*ahx-hx.*az);

dn = m.*(bx.*ahx-hx.*ax)./(m2.*bz.*ahx-hx.*az);

result = [an; bn; cn; dn];
```